Stapp Car Crash Journal, Vol. 68, pp. 14-30

Effect of A-Pillar Blind Spots on a Driver's Pedestrian Visibility during Vehicle Turns at an Intersection

Yasuhiro Matsui
National Traffic Safety and Environment Laboratory, Japan

Shoko Oikawa
Tokyo Metropolitan University, Japan

ABSTRACT – This study aims to elucidate the impact of A-pillar blind spots on drivers' visibility of pedestrians during left and right turns at an intersection. An experiment was conducted using a sedan and a truck, with a professional test driver participating. The driver was instructed to maintain sole focus on a designated pedestrian model from the moment it was first sighted during each drive. The experimental results revealed how the blind spots caused by A-pillars occur and clarified the relationship between the pedestrian visible trajectory distance and specific vehicle windows. The results indicated that the shortest trajectory distance over which a pedestrian remained visible in the sedan was 17.6 m for a far-side pedestrian model during a right turn, where visibility was exclusively through the windshield. For the truck, this distance was 20.9 m for a near-side pedestrian model during a left turn, with visibility through the windshield of 9.5 m (45.5% of 20.9 m) and through the passenger-side window of 11.4 m (54.5% of 20.9 m). Additionally, we quantified the trajectory distances where pedestrians became invisible when the driver's view was obstructed by A-pillars. The sedan exhibited the highest invisibility rate at 46.1% for a far-side pedestrian model during a right turn, followed by the truck at 17.8% for the same model. These findings will be instrumental in developing new driving support systems aimed at enhancing visibility in situations where pedestrians are obscured by A-pillars.

KEYWORDS – Driver visibility, pedestrian safety, window type, A-pillar blind spots, turning vehicle, intersection.

INTRODUCTION

In 2022, Japan recorded 2610 traffic fatalities, with pedestrians accounting for 955 fatalities (37%) (ITARDA 2023). Therefore, implementing countermeasures against fatal crashes involving pedestrians is crucial for reducing overall traffic fatalities.

In vehicle-to-pedestrian fatal crashes in Japan, the most frequent vehicle maneuver was "traveling straight" when the vehicle impacted a pedestrian at speeds of 25 km/h or higher (Matsui and Oikawa 2019). Recently, automatic emergency braking (AEB) systems that detect pedestrians using sensors installed in vehicles have been developed and are already being installed (Shibata 2009; Kuzumaki 2009; Sekiguchi 2011; Makabe 2012; Siddiqui et al. 2020; Naikal 2021). Qian et al. (2019) analyzed the optimized braking strategy for AEB systems in vehicle-to-pedestrian crashes to prevent or reduce collision severity. Data from real-world crash analyses (Tharp and Tsongos 1977; Waiz et al. 1983; Cuerden et al. 2007; Oh et al. 2008; Anderson et al. 1997; Davis 2001; Rosen and Sander 2009; Kong and Yang 2010) and simulations (Page and Foret-Bruno 2005) indicate that reducing vehicle impact speed correlates with a decreased pedestrian fatality rate, highlighting the effectiveness of AEB systems at higher speeds. Studies have revealed that pedestrian fatality rates are less than 5% when vehicle impact speeds are 30 km/h or less (Matsui et al. 2013, 2016). Additionally, a speed reduction of 10 km/h significantly lowers the pedestrian fatality rate, even at speeds of 40 km/h or

Address correspondence to: Dr. Yasuhiro Matsui, National Traffic Safety and Environment Laboratory, Chofu city, Tokyo, 182-0012, Japan. Electronic mail: ymatsui@ntsel.go.jp

higher (Matsui et al. 2013, 2016). Based on these findings, Japan mandated the installation of AEB systems with pedestrian detection in new passenger vehicles seating up to nine and goods-carrying vehicles with a gross vehicle weight (GVW) of 3.5 tons or less starting in November 2021 (JASIC 2021).

In Japan, the most common configuration of fatal pedestrian crashes involving vehicles traveling at 24 km/h or less occurs during right turns, where vehicles travel on the left side of the road (Matsui and Oikawa 2019). Although less frequent, left turns also contribute to these fatal crashes (Matsui and Oikawa 2019).

When driving, A-pillars at the front of the vehicle can create blind spots in the driver's frontal view (Santos et al. 2019). One factor contributing to pedestrian-involved crashes during left or right turns is the potential obstruction of a driver's view by A-pillars. Additionally, there is limited research investigating the specific windows through which drivers view pedestrians while turning. Given the discrepancies that arise between perceived and actual obstructions in a driver's field of view even under similar obstruction angles, Ramu et al. (2013) studied an alternative method for measuring A-pillar blind spots beyond obstruction angles. The study showed the A-pillar obstruction ratio as an alternative method, i.e., the ratio between the completely obstructed area and the particular boundary area, which was derived from experiments using a test car and high-intensity LEDs simulating driver vision. Santos et al. (2019) measured A-pillar obstruction angles in 75 vehicles sold in South America, finding minimum and maximum driver-side obstruction angles of 8º and 15.3º, respectively. Obeidat et al. (2022) conducted a laboratory experiment using a parked vehicle to explore how driver-related factors—such as age, weight, waist circumference, torso angle, and eye-to-windshield distance—affect A-pillar obstruction angles. These studies focused on A-pillar obstruction angles in stationary vehicles. To consider dynamic conditions, Schindler and Piccinini (2021) investigated driver behavior when a large truck with a trailer turned right at an intersection of right-hand traffic roads, where a bicycle model went straight beside the large truck. They analyzed video data from a camera installed in the cabin to identify the windows through which the driver checked the bicycle model. However, they did not examine A-pillar blind spots. Consequently, no experimental studies have assessed the frequency and duration of pedestrian obstruction due to A-pillar blind spots during intersection turns.

Therefore, this study aims to elucidate the impact of A-pillar-induced blind spots on drivers' visibility of pedestrians in vehicles making left and right turns at intersections. The study employs two vehicle types: a sedan and a truck with a GVW of 7.5 tons or less (hereafter referred to simply as a truck).

METHODS

Participants

A single male participant, a professional test driver, took part in this experiment. His task was to drive the test vehicles, starting 220 m before the intersection, and approach using standard driving maneuvers. The participant operated two different vehicle types and observed a pedestrian model while executing left or right turns at an intersection. Throughout the driving task, the participant wore glasses equipped with a monocular camera to capture images of the pedestrian model. He was instructed to maintain continuous focus on the designated pedestrian model from the moment of first sighting during each maneuver. Additionally, the participant was directed to keep his head position consistent and to adjust it along the z-axis to track the pedestrian model with the monocular camera upon sighting. The experiment protocol received approval from the Ethics Committee of the National Traffic Safety and Environment Laboratory (NTSEL) in Japan, and informed consent was obtained from the participant involved in the study.

Test Vehicles

For this study, we utilized two vehicles: a sedan and a truck. Photographs of the vehicles used are presented in Figure 1. The sedan had a GVW of 1535 kg, while the truck weighed 4680 kg with a maximum loading capacity of 2000 kg. The wheelbases measured 2700 mm for the sedan and 2525 mm for the truck. Both vehicles were manufactured in Japan and featured right-hand driver's seats. This study specifically focused on the A-pillars located on both the driver's side (right-hand side in the vehicle cabin) and the passenger side.

Vehicle speed and trajectory distance were recorded using a Global Positioning System (GPS) receiver (VGVS SP5Ci, VIOS Inc.), mounted on the roofs of the vehicles. Additionally, brake pedal force was measured using load cells (LPR-C-03KNS15, Kyowa Electronic Instruments Inc.) installed on the brake pedal of each vehicle.

Dimensions of Intersection and Pedestrian Models

Figure 2 illustrates the dimensions of the intersection utilized in this experiment. In Japan, vehicles drive on the left-hand side of the road. The crosswalk measured 4000 mm in width and 7000 mm in length. At the intersection, one pedestrian model was positioned at each of four locations along the extensions of the crosswalk's center line, as shown in Figure 2.

From the driver's perspective before entering the intersection, the pedestrian models were categorized as a far-side pedestrian model and a near-side pedestrian model during each left turn (Far-Left Model and Near-Left Model) and right turn (Far-Right Model and Near-Right Model).

Two types of pedestrian models were employed in this study: a male model representing the far-side pedestrian and a female model for the near-side pedestrian. The male model stood at a height of 1730 mm with a shoulder width of 440 mm, while the female model was 1610 mm tall with a shoulder width of 360 mm. Both models wore dark blue jackets and remained stationary.

During the experiment, the driver was instructed to perform four specific driving maneuvers on separate passes through the test intersection. The driver focused solely on one designated pedestrian model while approaching and passing through the intersection. The first run targeted the Far-Left Model under left-turn conditions, followed by the Near-Left Model in the second run. The third and fourth runs focused on the Far-Right Model and Near-Right Model, respectively, under right-turn conditions. This approach facilitated an individual assessment of the driver's visibility of both far-side and near-side pedestrian models during left and right turns in both the sedan and truck.

To ensure controlled visibility conditions, multiple containers were placed on both sides of the road before the intersection. These containers initially obstructed the driver's view of the pedestrian models at the beginning of each trial, as depicted in Figure 3. As the vehicle approached the intersection, the pedestrian model became visible, emerging from behind the container.

Vehicle Trajectory Distances, Vehicle Traveling Speed, Locations of Visibility, and Pedestrian Visible Distances

Vehicle speed and position were measured by a single GPS receiver mounted on the roof of each vehicle. Using this positional data, the vehicle's position along the trajectory (trajectory distance) was measured, as illustrated in Figure 4. The trajectory distance zero point was defined as the location where the vehicle's front end aligned with the pedestrian crossing line, depicted in Figure 4.

As depicted in Figure 4, measurement location L1 corresponded to the entrance line of the intersection, while L0 aligned with the pedestrian crossing line at the center of the crosswalk. Laser sensors installed at the bottom center of each vehicle's front end accurately identified locations L1 and L0. Laser-reflecting plates, affixed with reflective tape on aluminum plates, were placed at these locations.

The point where the driver first gained visibility of the pedestrian model was designated as the location of visibility (LV), illustrated in Figure 5. Distances over which a pedestrian remained visible and invisible in the vehicle trajectory were measured from LV to L0. These distances were defined as the pedestrian visible distance and pedestrian invisible distance, respectively.

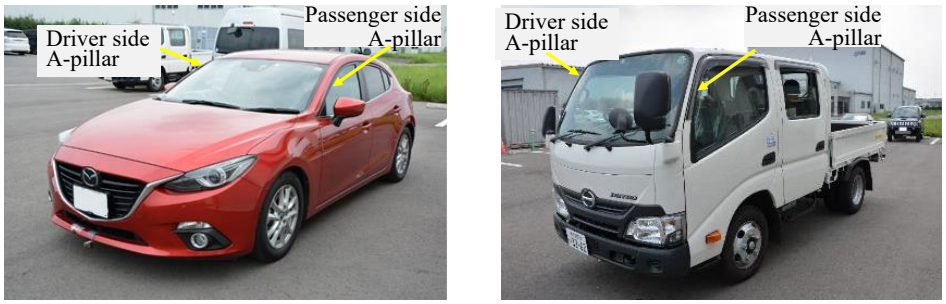

(a) Sedan (b) Truck

Figure 1. Photographs of the tested vehicles

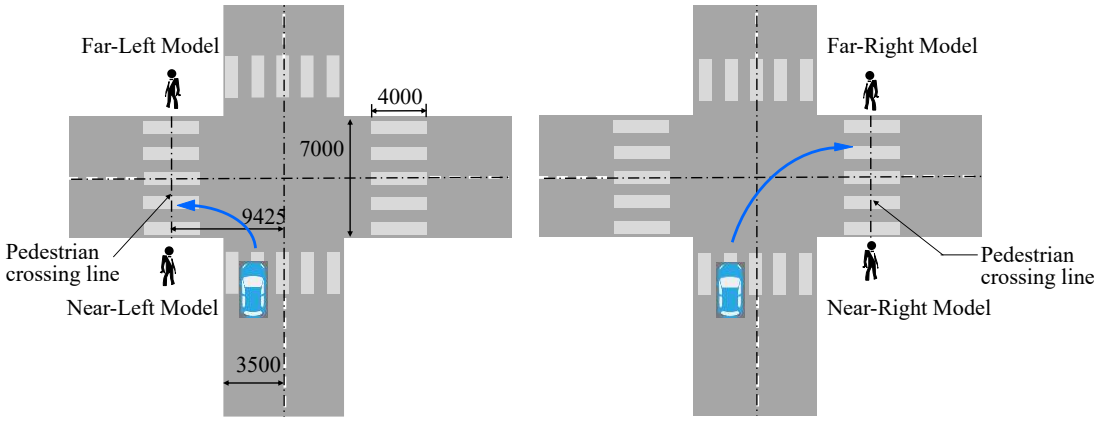

(a) Left turn (b) Right turn

Figure 2. Position of pedestrian models (unit: mm)

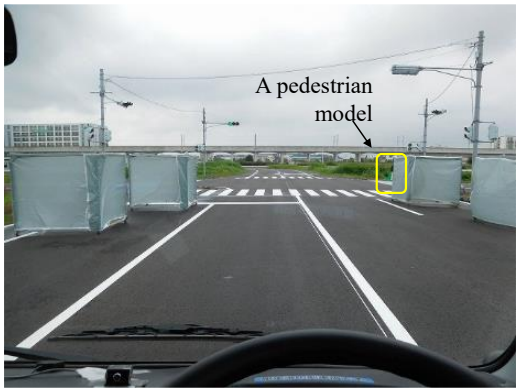

Figure 3. Containers placed near the intersection

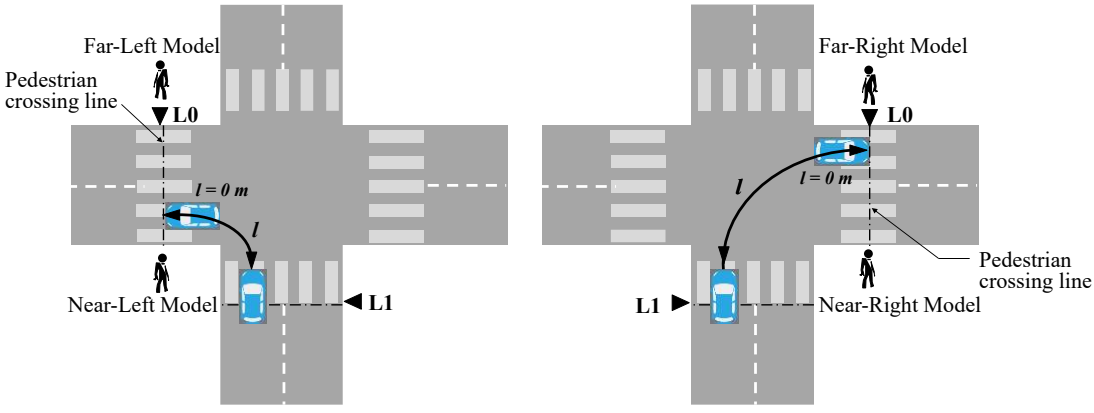

(a) Left turn (b) Right turn

Figure 4. Vehicle trajectory distance (*l*)

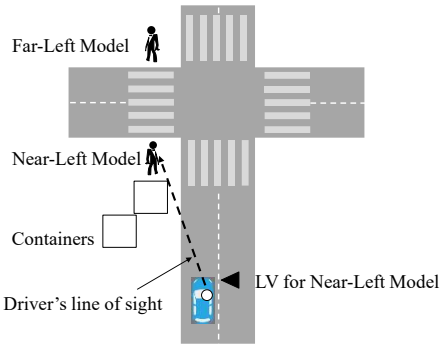

Figure 5. Location of visibility (LV), indicating the point where the driver began to see the pedestrian model while approaching the intersection

Figure 6. Glasses for the driver's line-of-sight measurement

Video Image Acquisition of Line-of-Sight

Glasses equipped with an eye-tracking device (Tobii Pro Glasses 2, Tobii Technology Inc.) (Figure 6) were used to record the frontal scene at 100 Hz (Tobii Technology 2016, 2018). These glasses featured a monocular camera to capture the driver's field of view and eye-tracking sensors to monitor eye gaze positions. The gaze information confirmed that the driver maintained focus on the pedestrian model as instructed. Examples of video scenes captured at LV, where the driver first observed the pedestrian model while driving a truck, are presented in Figure 7.

(1) Far-side pedestrian model

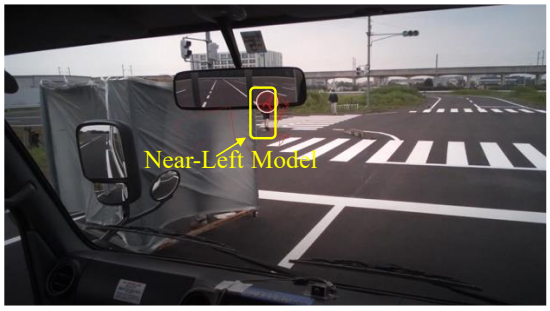

(2) Near-side pedestrian model

(a) Left-turn

(1) Far-side pedestrian model

(2) Near-side pedestrian model

(b) Right-turn

Figure 7. Examples of video scenes at the location of visibility (LV), demonstrating when the driver first observed the pedestrian model during a truck driving test

Analysis

This study's analysis focused on the interval between LV and L0, examining four key aspects:

1. Frequency and types of A-pillar obstructions: This included the number of occurrences and specific A-pillars (driver's side or passenger side) where the driver's view of pedestrian models was obstructed during each vehicle movement.

2. Relationships among trajectory, speed, pedal force, and visibility: The analysis explored correlations between vehicle trajectory distance, speed, pedal force, and the driver's visibility of pedestrian models.

3. Pedestrian visibility and window type: The study investigated the relationship between pedestrian visible trajectory distance and specific vehicle windows (driver's side, passenger's side, or windshield) through which the driver could observe pedestrian models.

4. Rates of pedestrian visibility/invisibility in LV–L0 movement: This part of the analysis examined both pedestrian visible and invisible trajectory distances in the LV–L0 driving segment to calculate visibility and invisibility rates.

Frequency and Types of A-Pillar Obstructions.

We analyzed the instances where drivers' view of pedestrian models was obstructed by A-pillars, identifying whether the obstruction occurred at the driver's side or passenger side A-pillar. This analysis covered the vehicle trajectory distance from LV to L0, utilizing images captured by the monocular camera of the wearable glasses. The driver's seat in the tested vehicles was positioned on the right side, placing the driver-side A-pillar on the right and the passenger-side A-pillar on the left from the driver's perspective.

Relationships Among Trajectory, Speed, Pedal Force, and Visibility.

Considering that the frequency of A-pillar obstructions is influenced by vehicle speed, we examined the relationships between vehicle trajectory distance, visibility of pedestrian models, vehicle speed, and pedal force during left or right turns at the intersection.

Relationship Between Pedestrian Visible Distance and Window Type.

We measured vehicle trajectory distance during which the pedestrian was visible/invisible (pedestrian visible/invisible trajectory distance). When the pedestrian was visible, we investigated through which vehicle window (driver's side, passenger's side, or windshield) visibility was achieved. The driver-side window was located on the right, while the passenger-side window was on the left.

Rates of Pedestrian Visibility/Invisibility in LV–L0 Driving.

Our focus extended beyond pedestrian visible trajectory distances to encompass pedestrian invisible trajectory distances in the LV–L0 segment. In numerous instances, the driver could not maintain continuous sight of the pedestrian model while driving from LV to L0. In such cases, visible or invisible trajectory distances were calculated as the cumulative length of each trajectory segment where the pedestrian model was visible or invisible, respectively. These measurements were used to determine the rates of pedestrian visibility/invisibility within the LV–L0 movement.

RESULTS

Frequency and Types of A-Pillar Obstructions

Table 1 presents the frequency and types of A-pillar obstructions that hindered the driver's view of pedestrian models during each vehicle movement from LV to L0. Figures 8 and 9 illustrate instances where the A-pillars of the sedan and truck obstructed the driver's view of pedestrian models during left turns at the intersection. The driver's view of the Far-Left Model was obstructed once by the driver-side A-pillar in both the sedan and truck. For the Near-Left Model, the view was obstructed once by the passenger-side A-pillar in both vehicles.

During right turns, the driver's view of the Far-Right Model was obstructed once by the driver-side A-pillar in the sedan and twice in the truck, as detailed in Table 1 and depicted in Figures 10 and 11. The driver's view of the Near-Right Model was obstructed once by the driver-side A-pillar in the sedan, with no obstruction observed in the truck.

Table 1. Frequency and types of A-pillars that obstructed pedestrian models when turning left and right

Turning direction	Pedestrian model	Number of times the view was obstructed by A-pillar		Types of A-pillars that obstructed the driver's view	
		Sedan	Truck	Sedan	Truck
Left	Far-Left	1	1	Driver side	Driver side
	Near-Left	1	1	Passenger side	Passenger side
Right	Far-Right	1	2	Driver side	Driver side
	Near-Right	1	—	Driver side	—

(a) Sedan

(b) Truck

Figure 8. Situations where the driver-side A-pillar obstructed the driver's visibility of a far-side pedestrian model during a left turn

(a) Sedan

(b) Truck

Figure 9. Situations where the passenger-side A-pillar obstructed the driver's visibility of a near-side pedestrian model during a left turn

(a) Sedan

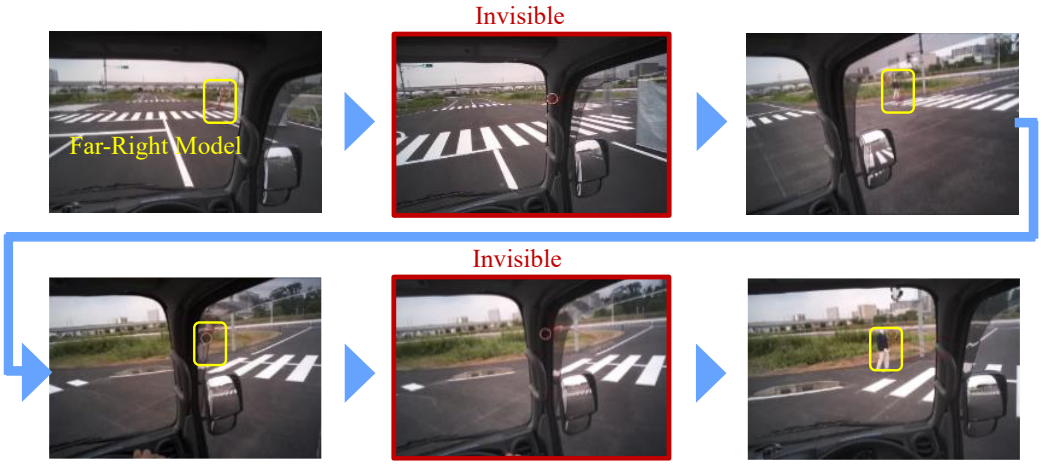

(b) Truck

Figure 10. Situations where the driver-side A-Pillar obstructed the driver's visibility of a far-side pedestrian model during a right turn

(a) Sedan

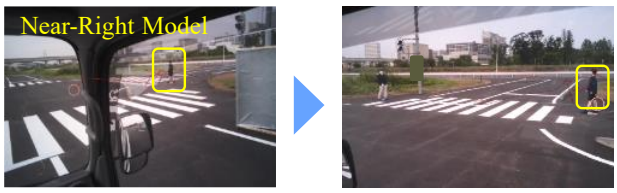

(b) Truck

Figure 11. Situations where the driver-side A-pillar obstructed the driver's visibility of a near-side pedestrian model during a right turn

Relationship Among Vehicle Trajectory Distance, Speed, Pedal Force, and Pedestrian Visibility

Figures 12 and 13 illustrate the relationship among vehicle trajectory distance, vehicle speed, pedal force, and pedestrian visibility. The driver began driving 220 m before L1, accelerating to approximately 40 km/h on a straight road, then applied approximately 20 N of pedal force to reduce speed when approaching the intersection. The center position of the crosswalk at the exit was set at 0 m.

Under left-turn conditions, the driver in the sedan first spotted the Far-Left Model at 25.9 m and the Near-Left Model at 21.8 m. In the truck, these distances were 26.6 m for the Far-Left Model and 22.5 m for the Near-Left Model.

During right-turn conditions, as shown in Figure 13, the sedan driver first sighted the Far-Right Model at 32.7 m and the Near-Right Model at 30.0 m. For the truck, these distances were 34.6 m for the Far-Right Model and 27.0 m for the Near-Right Model.

Regarding pedestrian invisibility, during right turns, the sedan driver could not see the Far-Right Model between 23.2 m and 8.1 m. In the truck, the pedestrian invisible trajectory distances for the Far-Right Model were from 26.2 m to 21.1 m and from 7.6 m to 6.5 m. A-pillar obstructions, particularly from the driver side, caused these limitations in both vehicles.

Table 2 details the vehicle speeds at LV, L1, and L0. Under left-turn conditions at LV, the sedan's speed (29.6 km/h) exceeded the truck's (23.3 km/h) when viewing the Far-Left Model. Under right-turn conditions at LV, the sedan's speed (37.3 km/h) was higher than the truck's (22.0 km/h). Similar trends were observed at L1 and L0 under both left and right-turn conditions.

Table 3 outlines the pedestrian visible trajectory distances in the LV–L0 and L1–L0 sections. In the LV–L0 section, the sedan exhibited shorter pedestrian visible trajectory distances than the truck in all conditions except for right turns while viewing the Near-Right Model. In the L1–L0 section, this trend persisted except under left-turn conditions while viewing the Near-Left Model.

Table 2. Vehicle speeds at LV, L1, and L0

Location	Vehicle velocity [km/h]											
	Left turn						Right turn					
	Far-Left Model			Near-Left Model			Far-Right Model			Near-Right Model		
	Sedan (a)	Truck (b)	Difference (a)-(b)	Sedan (a)	Truck (b)	Difference (a)-(b)	Sedan (a)	Truck (b)	Difference (a)-(b)	Sedan (a)	Truck (b)	Difference (a)-(b)
LV	29.6	23.3	6.3	20.9	21.0	-0.1	37.3	22.0	15.3	37.4	21.0	16.4
L1	21.9	18.0	3.9	16.6	16.4	0.2	21.1	18.3	2.8	20.3	16.3	4.0
L0	11.0	8.9	2.1	11.1	8.5	2.6	15.3	12.4	2.9	16.6	8.5	8.1

Table 3. Pedestrian visible trajectory distances in the LV–L0 and L1–L0 sections

Distance	Pedestrian visible trajectory distance [m]											
	Left turn						Right turn					
	Far-Left Model			Near-Left Model			Far-Right Model			Near-Right Model		
	Sedan (a)	Truck (b)	Difference (a)-(b)	Sedan (a)	Truck (b)	Difference (a)-(b)	Sedan (a)	Truck (b)	Difference (a)-(b)	Sedan (a)	Truck (b)	Difference (a)-(b)
LV–L0	25.9	26.6	-0.7	21.8	22.5	-0.7	32.7	34.6	-1.9	30.0	27.0	3.0
L1–L0	13.7	14.1	-0.4	14.6	14.3	0.3	19.5	20.6	-1.1	19.5	20.7	-1.2

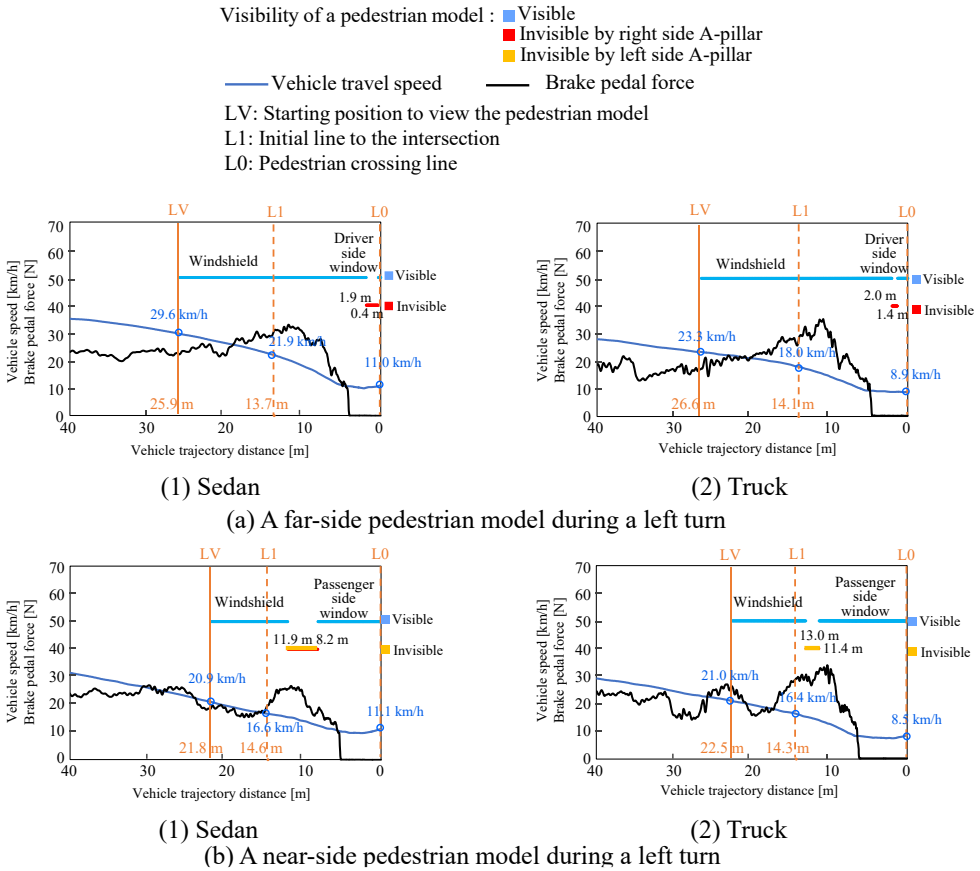

(1) Sedan (2) Truck

(a) A far-side pedestrian model during a left turn

(1) Sedan (2) Truck

(b) A near-side pedestrian model during a left turn

Figure 12. Relationship among vehicle trajectory distance, vehicle speed, pedal force, and visibility of a pedestrian model during a left turn

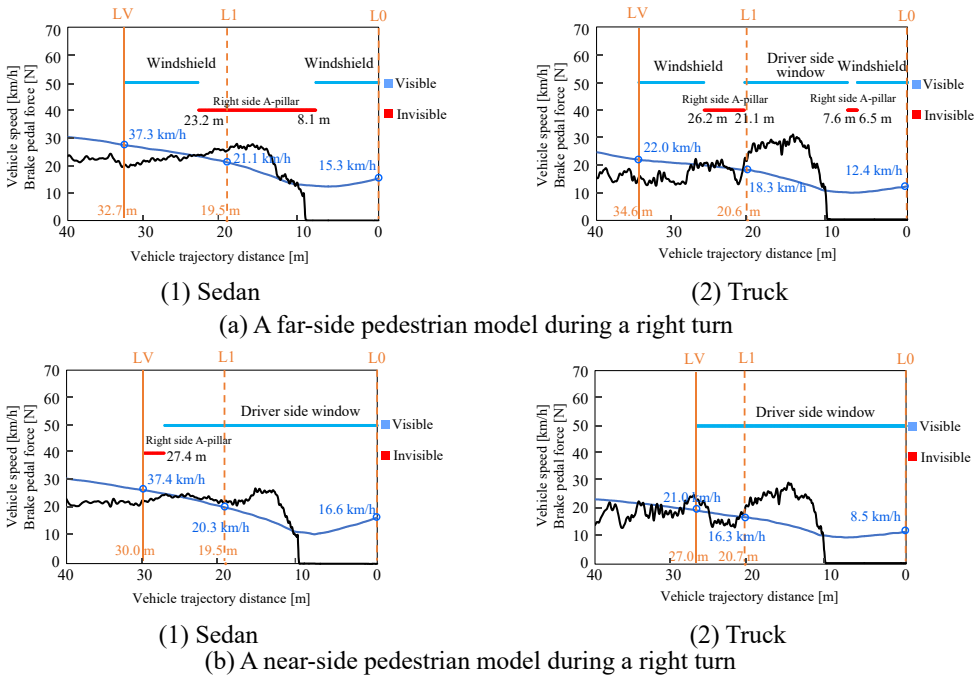

(1) Sedan (2) Truck

(a) A far-side pedestrian model during a right turn

(1) Sedan (2) Truck

(b) A near-side pedestrian model during a right turn

Figure 13. Relationship among vehicle trajectory distance, vehicle speed, pedal force, and visibility of a pedestrian model during a right turn

Relationship Between Pedestrian Visible Trajectory Distance and Vehicle Window Types

Figure 14 illustrates the pedestrian visible trajectory distances categorized by the types of vehicle windows through which the driver could observe the pedestrian models. Under left-turn conditions for the Far-Left Model, the pedestrian visible trajectory distances were 24.4 m in the sedan and 26.0 m in the truck. In the sedan, visibility of the Far-Left Model primarily occurred through the windshield (24.0 m, 98.4%) and minimally through the driver-side window (0.4 m, 1.6%). Similarly, in the truck, visibility of the Far-Left Model was through the windshield (24.6 m, 94.6%) and the driver-side window (1.4 m, 5.4%). These findings indicate that during left-turn conditions, drivers in both the sedan and truck predominantly observed the Far-Left Model through the windshield (94.6% to 98.4%).

For the Near-Left Model under left-turn conditions, the pedestrian visible trajectory distances were 18.1 m for the sedan and 20.9 m for the truck. In the sedan, visibility of the Near-Left Model was divided between the windshield (9.9 m, 54.7%) and the passenger-side window (8.2 m, 45.3%). Similarly, in the truck, visibility of the Near-Left Model was through the windshield (9.5 m, 45.5%) and the passenger-side window (11.4 m, 54.5%). Thus, under left-turn conditions, drivers in both vehicles experienced nearly equal visibility rates between the windshield and passenger-side window for the Near-Left Model.

For the Far-Right Model under right-turn conditions, the pedestrian visible trajectory distances were 17.6 m in the sedan and 28.4 m in the truck. The sedan driver viewed the Far-Right Model solely through the windshield, whereas in the truck, visibility was through the windshield (14.9 m, 52.5%) and the driver-side window (13.5 m, 47.5%).

Regarding the Near-Right Model under right-turn conditions, the pedestrian visible trajectory distances were 27.4 m in the sedan and 27.0 m in the truck, with visibility exclusively through the driver-side window in both vehicles.

In all conditions, the shortest pedestrian visible trajectory distance in the sedan was 17.6 m for the Far-Right Model during right turns, followed by 18.1 m for the Near-Left Model during left turns. In the truck, the shortest visible trajectory distance was 20.9 m for the Near-Left Model during left turns, followed by 26.0 m for the Far-Left Model during left turns.

Rates of Pedestrian Visibility and Invisibility in the LV–L0 Movement

Figure 15 displays the total pedestrian invisible trajectory distances during the LV–L0 movement. Under left-turn conditions, the total invisible trajectory distances for the Far-Left Model were 1.5 m for the sedan and 0.6 m for the truck. For the Near-Left Model, these trajectory distances were 3.7 m for the sedan and 1.6 m for the truck. Thus, in both scenarios of Far-Left Model and Near-Left Model under left-turn conditions, the sedan exhibited longer pedestrian invisible trajectory distances than the truck. Additionally, for both vehicle types during left turns, the invisible trajectory distances for the Near-Left Model were greater than those for the Far-Left Model.

Under right-turn conditions, the total pedestrian invisible trajectory distances for the Far-Right Model were 15.1 m for the sedan and 6.2 m for the truck. For the Near-Right Model, these trajectory distances were 2.6 m for the sedan and nonexistent for the truck. Therefore, during both scenarios of Far-Right Model and Near-Right Model in right turns, the sedan exhibited longer invisible trajectory distances than the truck. Moreover, for both vehicle types during right turns, the invisible trajectory distances for the Far-Right Model exceeded those for the Near-Right Model.

Figure 16 illustrates the rates of pedestrian visibility and invisibility during the LV–L0 movement. Under left-turn conditions, the invisibility rates for the Far-Left Model were 5.9% in the sedan and 2.3% in the truck. For the Near-Left Model, these rates were 17.0% in the sedan and 7.2% in the truck. For both the Far-Left Model and Near-Left Model, the invisibility rates were slightly higher in the sedans than in the trucks.

Under right-turn conditions, the invisibility rates for the Far-Right Model were 46.1% in the sedan and 17.8% in the truck. For the Near-Right Model, these rates were 8.7% in the sedan and 0.0% in the truck. In both scenarios of Far-Right Model and Near-Right Model, the sedans had higher invisibility rates than the trucks. Furthermore, for both vehicle types during right turns, the invisibility rates for the Far-Right Model were slightly higher than those for the Near-Right Model.

Among the invisibility rates for left and right turns, the highest rate was observed in the sedan for the Far-Right Model during right turns (46.1%), followed by 17.8% for the truck under the same condition, and

17.0% for the sedan for the Near-Right Model during left turns.

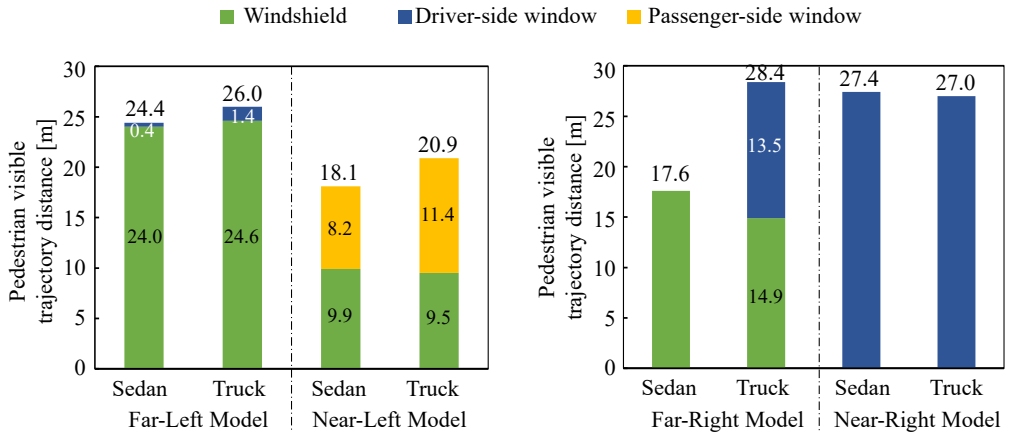

(a) Left turn (b) Right turn

Figure 14. Pedestrian visible trajectory distances by vehicle window type

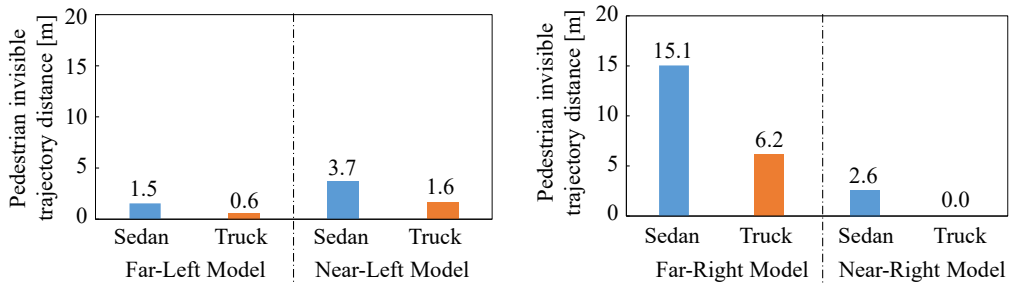

(a) Left turn (b) Right turn

Figure 15. Total pedestrian invisible trajectory distances in the LV–L0 movement

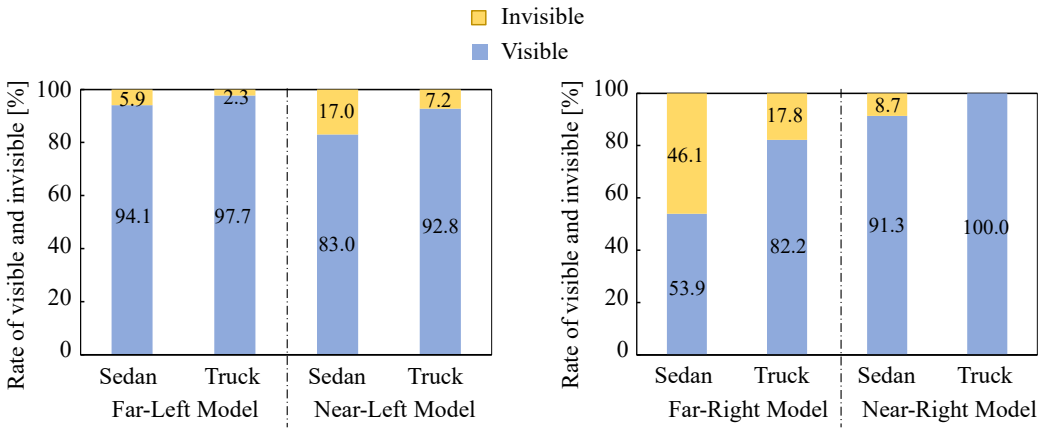

(a) Left turn (b) Right turn

Figure 16. Rates of pedestrian visible/invisible trajectory distances in the LV–L0 movement

DISCUSSION

The experimental findings from right turns made by the sedan revealed a pedestrian invisibility rate of 46% for the Far-Right Model. This indicates that drivers may encounter difficulty observing pedestrian models for approximately half of the vehicle trajectory distance in the LV–L0 section. Hashimoto et al. (2009) examined blind spot areas caused by A-pillars during right turns at an intersection using ground plane projection maps. Their research demonstrated that pedestrians crossing from left to right at an intersection tended to remain in the blind spot longer compared to those crossing in the opposite direction. Such findings suggest that fatal pedestrian crashes involving vehicles making right turns at low speeds are frequently reported in real-world scenarios (Matsui and Oikawa 2019). One potential contributing factor could be delays in drivers' cognitive responses to pedestrians due to A-pillar obstructions.

In both left and right turns, the sedan consistently exhibited higher invisibility rates compared to the truck, as depicted in Figure 16. Particularly noteworthy is the sedan's invisibility rate for the Far-Right Model (46%), significantly surpassing that of the truck (18%) during right turns. This discrepancy may be partially attributed to differences in the inclination angles of the A-pillars. In the vehicles tested, the sedan featured an A-pillar inclination angle of 29°, whereas the truck had an angle of 60°, as illustrated in Figure 17. The sedan's smaller inclination angle from the horizontal line could allow for longer trajectory distances of invisibility for drivers during intersection turns. Additionally, structural disparities in the A-pillars between the two vehicles may also play a role; the sedan's A-pillar was wider compared to that of the truck, as shown in Figure 11. A-pillars are designed to safeguard occupants in frontal collisions and rollovers, with sedans typically incorporating sturdier A-pillars to enhance protection. Consequently, the combination of a smaller inclination angle and thicker A-pillar in sedans might lead to extended invisible trajectory distances for far-side pedestrian models.

The eyepoint heights of the tested vehicles were 1196 mm from the ground for the sedan and 1693 mm for the truck. Despite the truck having an eyepoint height 497 mm higher, the impact on the driver's view being obstructed by the A-pillar is likely minimal, as the A-pillar angle remains relatively constant regardless of eyepoint height.

In this study, we analyzed pedestrian visible trajectory distances concerning the types of vehicle windows through which drivers could observe pedestrian models, as shown in Figure 14. Under left-turn conditions, drivers could see the Near-Left Model through both the windshield and the passenger-side window at roughly equal rates for both the sedan and the truck. Initially, drivers view the Near-Left Model through the windshield. As the vehicle approaches the intersection, however, drivers may fail to recognize the Near-Left Model unless they shift their gaze to the passenger-side window. In typical traffic situations, drivers often focus primarily on oncoming traffic participants such as cyclists through the windshield while approaching an intersection. Consequently, identifying a near-side pedestrian in such scenarios could be challenging unless drivers intentionally glance through the passenger-side window.

(a) Sedan (b) Truck

Figure 17. Inclination angles of A-pillars from the horizontal line

Our investigation also considers pedestrian positions under right-turn conditions, given that most vehicle-to-pedestrian collisions at low speeds in real-world crashes occur during this maneuver (Matsui et al. 2019). The Institute for Traffic Accident Research and Data Analysis of Japan (ITARDA) categorizes total road width into several groups for documenting real-world crashes. The full road width (7.0 m) in our experimental setup corresponds to the 5.5–13 m road width category in ITARDA's classification. According to ITARDA's database, within this road width range, right-turn vehicle collisions involving far-side pedestrians accounted for 47%, while those involving near-side pedestrians were 53% (ITARDA 2012). This indicates a slightly higher incidence of crashes involving near-side pedestrians. In our study, we observed that during right turns, the near-side pedestrian was visible only through the driver-side window. Viewing through the driver-side window, rather than through the windshield, requires drivers to turn their heads to the right. One contributing factor to such crashes may be the challenge of monitoring near-side pedestrians through the driver-side window rather than through the windshield.

Examining vehicle travel speed and pedal force during left turns, we observed that the driver released the brake pedal, reducing the pedal force to 0 N, and subsequently began accelerating the vehicle. During acceleration in both tested vehicles, the driver's view of the Far-Left Model was obstructed by the A-pillar, as shown in Figure 12. The locations of this obstruction ranged from 1.9 m to 0.4 m in the sedan and 2.0 m to 1.4 m in the truck along the trajectory distance, corresponding to a time to collision (TTC) of 0.64 s to 0.12 s in the sedan and 0.83 s to 0.55 s in the truck. In this study, TTC is defined as the real time to reach the location at the center line of the pedestrian crosswalk (L0) (e.g., 0.64 s corresponds to the time before reaching L0). The location of 1.9 m or 2.0 m from L0 corresponds to the edge of the crosswalk. Our analysis suggests that when a vehicle accelerates, driver visibility is obstructed near the edge of the crosswalk due to A-pillar obstructions. In these left-turn scenarios, there is a potential risk of collisions with far-side pedestrians. Thus, the development of sensing technologies that alert drivers to approaching pedestrians between left-turning vehicles and far-side pedestrians is imperative.

For instance, when the sedan turned right, the Far-Right Model became visible to the driver at a vehicle trajectory distance of 32.7 m but was obscured from 23.2 m to 8.1 m before becoming visible again at 8.1 meters. The 8.1 m mark approximately corresponds to the center of the intersection, near the crosswalk. If a driver, distracted by other traffic participants during a right turn, fails to notice a pedestrian appearing at the center of the intersection, there is a risk of a vehicle-to-pedestrian collision. As a technological countermeasure, research using vehicle-to-everything (V2X) communication technology is underway (Cornec et al. 2023). Additionally, the development of vehicles capable of directly detecting pedestrians on crosswalks using cameras or lasers and subsequently applying automatic braking is anticipated. There is an urgent need for new driver-assist technologies that can recognize pedestrians even when they are outside the driver's field of view.

In this experiment, we investigated how the A-pillar blind spot occurs with a stationary pedestrian model. When a pedestrian model moves, the obstruction of a driver's view by the A-pillar may differ from the findings of this study. This difference could depend on the relative positions of a moving pedestrian model and the A-pillar in a turning vehicle (Hashimoto et al. 2009). In the present experiment, during right turns with the sedan, the driver-side A-pillar obstructed the driver's visibility of the Far-Right Model, as depicted in Figure 10(a). The sedan exhibited an invisible trajectory distance of 15.1 m, ranging from 23.2 m to 8.1 m in the LV–L0 section. If a pedestrian model begins crossing just before the vehicle reaches the point at 8.1 m along its trajectory distance, the model may remain in the blind spot area longer as the vehicle completes the turn. In such scenarios, the distance at which the model becomes visible again will be less than 8.1 m. Considering this scenario in real traffic conditions, the shorter visibility distance increases the risk of a pedestrian-involved collision. In future studies, it is crucial to investigate at which position on a crosswalk pedestrians become invisible due to an A-pillar in conjunction with vehicle movements.

We utilized different sizes of pedestrian models for far-side and near-side scenarios. For instance, the dimensions from median to shoulder were 220 mm for male and 180 mm for female dummies. The width of the pedestrian model can affect when view obstruction by the A-pillar begins for the driver. Therefore, future research should explore how varying pedestrian sizes influence pedestrian visible trajectory distances, particularly for far-side and near-side scenarios.

There have been various methods focused on addressing blind spots caused by A-pillars. Many studies have targeted obstruction angles or invisibility angles using parked vehicles (Sundin and Hasselblad 2008; Ramu et al. 2013; Santos et al. 2019; Obeidat et al. 2022). Ramu et al. (2013) conducted a laboratory experiment using LEDs instead of a driver's eyes, while Obeidat et al. (2022) gathered experimental data where participants in parked vehicles used smartphone cameras to measure invisibility angles caused by pillars. However, to date, there is no literature specifically targeting A-pillar blind spots related to pedestrians using experimental data from camera images at a driver's eye level while a vehicle is in motion on the road. In contrast, studies utilizing Japanese near-miss databases recorded by drive recorder cameras, provided by the Smart Mobility Research Center of Tokyo University of Agriculture and Technology, analyze driver behavior in actual traffic environments (Matsui and Oikawa 2023; Raksincharoensak et al. 2010). These recorders are installed near the front mirror, differing from the driver's eye position. Therefore, the methodology and findings of this study represent a novel contribution to the field of ergonomics.

This research does have several limitations. The experiment involved one professional driver who was 186 cm tall, using glasses equipped with a camera for image capture and analysis. If a driver is taller than 186 cm, they may adjust their seat farther back from the steering wheel than the test driver, resulting in different eye points and potential variations in A-pillar blind spots. Obeidat et al. (2022) investigated factors affecting invisibility angles caused by vehicle pillars, highlighting that the distance between a driver's eyes and the windshield is a significant factor. They noted that taller participants tend to position their driver seats farther back from the steering wheel, while shorter individuals show the opposite trend. Further investigation into A-pillar obstruction across a wide range of driver eye positions considering different human dimensions—including age, gender, stature, weight, chest size, and waist circumference—is necessary to deepen our understanding.

Our study investigated driver visibility during turning movements using only a sedan and a truck, which limited the variety of vehicles tested. Even within sedan types, the angle and cross-section thickness of A-pillars can vary between vehicles. Ramu et al. (2013) conducted experiments using high-intensity LEDs instead of a driver's eyes and a stationary vehicle in the test site, demonstrating that different A-pillar obstruction angles resulted in varying obstruction rates. Additionally, the height of the cabin can be greater in heavier truck GVWs, potentially altering visibility of pedestrians due to the higher position of the driver's eyes. Further investigations into driver view across a broader spectrum of vehicle types and models are necessary.

CONCLUSIONS

This study investigated the impact of A-pillar blind spots on a driver's visibility of pedestrians during left and right turning movements at intersections, using two types of vehicles: a sedan and a truck with a GVW of 7.5 tons or less. A professional male test driver participated in the experiment, wearing glasses equipped with a monocular camera to capture images. The driver was instructed to maintain focus solely on a targeted pedestrian model from the moment it was first sighted under each condition. The primary focus of the analysis was the vehicle trajectory distance from the location of visibility (LV), where the driver first spotted the pedestrian model, to the location of the pedestrian crossing line (L0).

The experimental results specifically revealed how A-pillar blind spots occurred and clarified the relationship between pedestrian visible trajectory distance and specific vehicle windows. The findings indicated that the shortest pedestrian visible trajectory distance for the sedan was 17.6 m for the far-side pedestrian model (Far-Right Model) during a right turn, with visibility solely through the vehicle's windshield. For the truck, the shortest pedestrian visible trajectory distance was 20.9 m for the near-side pedestrian model (Near-Left Model) during a left turn; visibility for this model was achieved through the windshield for 9.5 m (45.5% of 20.9 m) and through the passenger-side window for 11.4 m (54.5% of 20.9 m).

Additionally, we calculated the pedestrian invisible trajectory distances when the driver's view was obstructed by A-pillars. The sedan exhibited the highest rate of pedestrian invisibility at 46.1% for the Far-Right Model during a right turn, followed by the truck at 17.8% for the Far-Right Model under similar conditions.

Considering the impact of A-pillar blind spots on driver visibility during vehicle turning maneuvers, there is a clear need to develop new driver support systems. These systems should be capable of identifying pedestrians at risk of collisions, especially when the driver's direct line of sight is obstructed. The findings from this study will aid in the development of new driving support systems aimed at improving visibility in situations where pedestrians are obscured by A-pillars.

ACKNOWLEDGMENTS

This research was funded by the Ministry of Land, Infrastructure, Transport, and Tourism (MLIT) of Japan, in 2019. The authors are grateful to Mr. Masashi Narita of NTSEL, Japan, for his support in conducting the current analysis.

REFERENCES

Anderson, R.W.G., McLean, A.J., Farmer, M.J.B., Lee, B.H., and Brooks, C.G. (1997) Vehicle travel speeds and the incidence of fatal pedestrian crashes. Accident Analysis & Prevention 29(5): 667-674.

Cornec, L., Unger, T., Feifel. H., Hermitte, T., Puller, N., and Mousavi, M. (2023) Analysis of the European car road crashes for the identification of the main use cases for a significant road safety improvement through V2X. Proc. 27th International Technical Conference on the Enhanced Safety of Vehicles (ESV), Yokohama, Japan, 4–6 April 2023.

Cuerden, R., Richards, D., and Hill, J. (2007) Pedestrians and Their Survivability at Different Impact Speeds. Proc. 20th International Technical Conference on the Enhanced Safety of Vehicles, Lyon, France, 18–21 June 2007.

Davis, G. (2001) Relating severity of pedestrian injury to impact speed in vehicle-pedestrian crashes. Transportation Research Record 1773(1): 108-113.

Hashimoto, H., Hosokawa, T., Suzuki, T., and Miki, Y. (2009) Simulation methods of the direct field of view for turn right situation at different scale intersections. Journal of Society of Automotive Engineers of Japan 40(3): 891-897 (in Japanese).

ITARDA (2012) Institute for Traffic Accident Research and Data Analysis of Japan (ITARDA) Information No. 95, 95 (in Japanese).

ITARDA (2023) Annual Traffic Accident Report in 2022. Institute for Traffic Accident Research and Data Analysis of Japan (ITARDA), Tokyo, Japan, (in Japanese).

JASIC. Test for advanced emergency braking systems of passenger motor vehicle, etc., TRIAS12-R152-01. Automobile Type Approval Handbook for Japanese Certification; Japan Automobile Standards Internationalization Center (JASIC): Tokyo, Japan. Available online: https://www.jasic.org/e/index_e.htm.

Kong, C., and Yang, J. (2010) Logistic regression analysis of pedestrian casualty risk in passenger vehicle collisions in China. Accident Analysis & Prevention 42(4): 987-993.

Kuzumaki, S. (2009) Our approach to a safe sustainable society. Journal of Society of Automotive Engineers of Japan 63(12): 11-19 (in Japanese).

Makabe, S. (2012) Active safety system new eyesight version 2. Journal of Society of Automotive Engineers of Japan 66(3): 88-93 (in Japanese).

Matsui, Y., and Oikawa, S. (2019) Situational characteristics of fatal pedestrian accidents involving vehicles traveling at low speeds in Japan. Traffic Injury Prevention 20(sup1): S1-S6.

Matsui, Y., and Oikawa, S. (2023) Characteristics of dangerous scenarios between vehicles turning right and pedestrians under left-hand traffic. Applied Science, open access 13.

Matsui, Y., Oikawa, S., and Ando, K. (2013) Risks of pedestrian serious injuries and fatalities associated with impact velocities of cars in car-versus-pedestrian accidents in Japan. SAE Technical Paper 2013-22-0008.

Matsui, Y., Oikawa, S., Sorimachi, K., Imanishi, A., and Fujimura, T. (2016) Association of impact velocity with risks of serious injuries and fatalities to pedestrians in commercial truck–pedestrian accidents. SAE Technical Paper 2016-22-0007.

Naikal, N. (2021) Improving pedestrian automatic emergency braking. SAE Technical Paper 2021-01-1008.

Obeidat, S. M., Altheeb, F. N., Momani, A., and Theeb, A. N. (2022) Analyzing the invisibility angles formed by vehicle blind spots to increase driver's field of view and traffic safety. International Journal of Occupational Safety and Ergonomics 28(1), 129–138.

Oh, C., Kang, Y., and Kim, W. (2008) Assessing the safety benefits of an advanced vehicular technology for protecting pedestrians. Accident Analysis & Prevention 40(3): 935-942.

Page, Y., and Foret-Bruno, J. (2005) Are expected and observed effectiveness of emergency brake assist in preventing road injury accidents consistent? Proc. 19th International Technical Conference on the Enhanced Safety of Vehicles, Washington, D.C., U.S., 6–9 June 2005.

Qian, Y., Yang, X., Xiao, L., and Zhu, Y. (2019) Optimization of braking strategy for automatic emergency braking system in vehicle-pedestrian accidents. SAE International Journal of Passenger Cars-Electronic and Electrical Systems 12: 117-128.

Raksincharoensak, P., Tago, M., Nagai, M., Mizoguchi, Y., Sasaki, K. (2010) Analysis on environmental hazard and safety confirmation in right turn behavior using continuous sensing derive recorder. Journal of Society of Automotive Engineers of Japan 41(4): 909-914 (in Japanese).

Ramu, B., Khurana, R., and Sharma, P. (2013) An alternate methodology to measure the A-pillar obstruction in passenger cars. SAE Technical Paper 2013-26-0030.

Rosen, E., and Sander, U. (2009) Pedestrian fatality risk as a function of car impact speed. Accident Analysis & Prevention 41(3): 536-542.

Santos, A., Gerez, A., Pádua, A., Genaro, P., Silva, R., and Ferreira, S. (2019) The influence of A-pillar obscuration/location on driver visibility, SAE Technical Paper 2019-36-0062.

Schindler, R., and Piccinini, G. B. (2021) Truck drivers' behavior in encounters with vulnerable road users at intersections: Results from a test-track experiment. Accident Analysis & Prevention 159.

Sekiguchi, M. (2011) Introduction of SUBARU Advanced Driving System "EyeSight ver.2". Proc. Safety Engineering Symposium, The Japan Society of Mechanical Engineers, Tokyo, Japan, 7 July 2011 (in Japanese).

Shibata, E. (2009) Development of driving assist system "EyeSight" by new stereo camera. Journal of Society of Automotive Engineers of Japan 63(2): 93-98 (in Japanese).

Siddiqui, O., Famiglietti, N., Nguyen, B., Hoang, R., and Landerville, J. (2020) Empirical study of the braking performance of pedestrian autonomous emergency braking (P-AEB). SAE Technical Paper 2020-01-0878.

Smart Mobility Research Center, Mechanical Systems Engineering, Tokyo University of Agriculture and Technology, Available online: https://web.tuat.ac.jp/~smrc/about.html.

Sundin, A., and Hasselblad, H. (2008) Visibility driven design of new modularized Volvo car tophat structure. SAE Technical Paper 2008-36-0126.

Tharp, K., and Tsongos, N. (1977) Injury severity factors-traffic pedestrian collisions. SAE Technical Paper 770093.

Tobii Technology, Tobii Pro Glasses 2 User's manual (2016) Available online: https://go.tobii.com/Glasses2UM

Tobii Technology, Tobii Pro Glasses 2 Product description (2018) Available online: https://nbtltd.com/wp-content/uploads/2018/05/tobiiproproductdescription.pdf.

Waiz, F., Hoefliger, M., and Fehlmann, W. (1983) Speed limit reduction from 60 to 50 km/h and pedestrian injuries. SAE Technical Paper 831625.